# Rheological Properties of Living Cytoplasm: Endoplasm of *Physarum* Plasmodium

MASAHIKO SATO, TERENCE Z. WONG,* and ROBERT D. ALLEN
*Department of Biological Sciences, and *Thayer School of Engineering, Dartmouth College, Hanover, New Hampshire 03755*

ABSTRACT Magnetic sphere viscoelastometry, video microscopy, and the Kamiya double chamber method (Kamiya, N., 1940, *Science* [*Wash. DC*], 92:462–463.) have been combined in an optical and rheological investigation of the living endoplasm of *Physarum polycephalum*. The rheological properties examined were yield stress, viscosity (as a function of shear), and elasticity. These parameters were evaluated in directions perpendicular; (*X*) and parallel (*Y*) to the plasmodial vein. Known magnetic forces were used for measurements in the *X* direction, while the falling ball technique was used in the *Y* direction (Cygan, D. A., and B. Caswell, 1971, *Trans. Soc. Rheol.* 15:663–683; MacLean-Fletcher, S. D., and T. D. Pollard, 1980, *J. Cell Biol.*, 85:414–428).

Approximate yield stresses were calculated in the *X* and *Y* directions of 0.58 and 1.05 dyn/cm$^2$, respectively. Apparent viscosities measured in the two directions ($\eta_x$ and $\eta_y$) were found to fluctuate with time. The fluctuations in $\eta_x$ and $\eta_y$ were shown, statistically, to occur independently of each other. Frequency correlation with dynamoplasmograms indicated that these fluctuations probably occur independently of the streaming cycle. Viscosity was found to be a complex function of shear, indicating that the endoplasm is non-Newtonian. Plots of shear stress vs. rate of shear both parallel and perpendicular to the vein, showed that endoplasm is not a shear thinning material.

These experiments have shown that living endoplasm of *Physarum* is an anisotropic viscoelastic fluid with a yield stress. The endoplasm appears not to be a homogeneous material, but to be composed of heterogeneous domains.

Previous investigations of living cytoplasm in its many states have been crude at best. Micromanipulation (9) and various centrifuge experiments (2, 8, 16, 19) have been informative, but disruptive to cell structure. One promising approach is the magnetic particle method (53). The pioneering attempts of Heilbronn (18) and Seifriz (50), along with the efforts of Crick and Hughes (10), Yagi (56), and Hiramoto (20) have been instrumental in the development of this technique. Although largely qualitative, these experiments have indicated that the cytoplasm of various systems is non-Newtonian. Therefore, cytoplasm can not be characterized by a single rheological parameter such as viscosity. Hiramoto's application (20) of the magnetic particle method in sea urchin eggs and Hwang's experiments (23) in mucus further established the possibility of calibrating the method.

We have developed a calibrated magnetic particle technique to analyze nondisruptively, yield stress, apparent viscosity, and elasticity, in living cytoplasm. It is designed to be applied to large syncytial systems, cell extracts, and fluid volumes of 10 μl or less. The technique has been successfully applied to the endoplasm of the large acellular slime mold, *Physarum polycephalum*. An abundance of biochemical, ultrastructural, and biophysical information is available on *Physarum* (see reviews: 15, 27, 28, 31, 35, 41). In addition, this material is easily cultured and manipulated. *Physarum* exhibits an important example of nonmuscular motility, shuttle streaming, which can be modulated with the double chamber method (26). The magnetic particle technique has been improved (see APPENDIX) and combined with video enhanced microscopy and the double chamber method. This combination makes possible the quantitative characterization of the rheological properties of living *Physarum* endoplasm. Portions of this

THE JOURNAL OF CELL BIOLOGY · VOLUME 97 OCTOBER 1983 1089-1097
© The Rockefeller University Press · 0021-9525/83/10/1089/09 $1.00

work have appeared in a preliminary account (49).

## MATERIALS AND METHODS

*Culture and Double Chamber Techniques:* An Albino strain of *Physarum polycephalum*, CH 975/943, was the generous gift of the late C. E. Holt, Massachusetts Institute of Technology. Axenic cultures were maintained by the method of Daniel and Baldwin (12) on peptone yeast extract culture media (7). Macroplasmodia were grown on dialysis membrane (12–14k cutoff, Spectrum Medical Industries, Inc., Los Angeles, CA) on peptone yeast extract agar dishes to facilitate handling of plasmodial veins.

*Physarum* macroplasmodia will phagocytize magnetic particles (see Appendix), but greater yield can be achieved in less time by pushing particles in with a glass needle. Plasmodial veins were sealed in 2% Low Gel Temperature Agarose (Sigma Chemical Co., St. Louis, MO) in the area occupied by the stopper in Fig. 1. This allowed the modulation of the pressure gradient across the two regions of the double chamber. The procedure for sample preparation has been described previously (49).

Cytoplasmic streaming of the endoplasm in the mounted specimen was observed through the microscope. When a suitable particle came into view, the streaming endoplasm was stopped by applying balance pressure. A manometer connected to one side of the double chamber monitored this pressure. The endoplasm was held motionless for ~30 s before measurements were taken, to minimize effects from possible shock resulting from the initial application of balance pressure.

*Video Microscopy:* A Zeiss WL microscope with sample holder serving as the mechanical stage was tilted 90° with an aluminum brace. Long working distance matched objectives (Zeiss UD 40/0.65, 6.9 mm WD) for either brightfield or polarized light microscopy were used with 12 W tungsten or HBO 100 W mercury vapor illumination (Fig. 2). The illuminating intensity was modulated with a second polarizer mounted above the field stop, and preceded by a 546-nm narrow band interference filter and an $H_2O$ infrared filter.

In brightfield observations, a MK II 65 video camera with Newvicon tube (Dage-MTI, Inc., Michigan City, IN) with auto/manual black, auto-gamma, and external sync. drive capabilities (24) was used. A second camera (model SC-15A, Sylvania Electric Products, Inc., Bedford, MA) was focused on the illuminated manometer. The MK II 65 camera was externally driven by the SC-15A camera through a video screen splitter/inserter (model V270SP, Vicon Industries, Inc., Plainview, NY). This enabled the video monitor to display simultaneously, balance pressure, magnetic current, microscopic field (110 $\mu$m wide), and time (Panasonic model WJ-810, H. B. Educational Systems, Inc., New Haven, CT), see Fig. 2.

For video-enhanced microscopy in polarized light, the C-1000-01 camera (Chalnicon tube, Hamamatsu Systems, Inc., Waltham, MA) with variable gain and offset was used to generate the video signal. This signal was further processed by the Frame Memory Image Analysis polyprocessor (model C1440-01, Hamamatsu Systems, Inc.) (4). De Sénarmont compensation (6) was used. As the specimen could not be rotated from its 0° orientation, the polarizer and $\lambda/4$ plate were set at −45°.

*Viscometry In Vivo:* The coordinate system ($X$, $Y$, $Z$) adopted for this presentation is detailed in Fig. 3. Magnetic spheres were manipulated in the $Y$ direction by adjusting the chamber pressure, and maneuvered in the $X$ direction by the electromagnets.

For a discussion of the theoretical basis of both falling ball and magnetic sphere viscometry used in the determination of yield stress and apparent viscosity, see Appendix.

## RESULTS

### Phagocytized Magnetic Particles

Magnetic particles in the endoplasm were enclosed in vacuoles. In clear specimens, the difference in refractive index between the vacuole interior and the endoplasm allowed visualization of the vacuolar membrane shear surface. Only tight fitting vacuolated spheres were used in the generation of rheological data.

### Video Polarized Light Microscopy

Prepared specimens in experimental conditions were stable under illumination for several hours. Opposite de Sénarmont compensated images were subtracted by the polyprocessor (Hamamatsu Systems, Inc.) (4) in an effort to enhance the visualization of the faint negative birefringence (BR)[1] of the endoplasm (43). Nevertheless, most of the contrast visible was not attributable to BR. In agreement with the observations of Nakajima and Allen (43), the negative BR of the endoplasm was found to be independent of the direction or velocity of shuttle streaming.

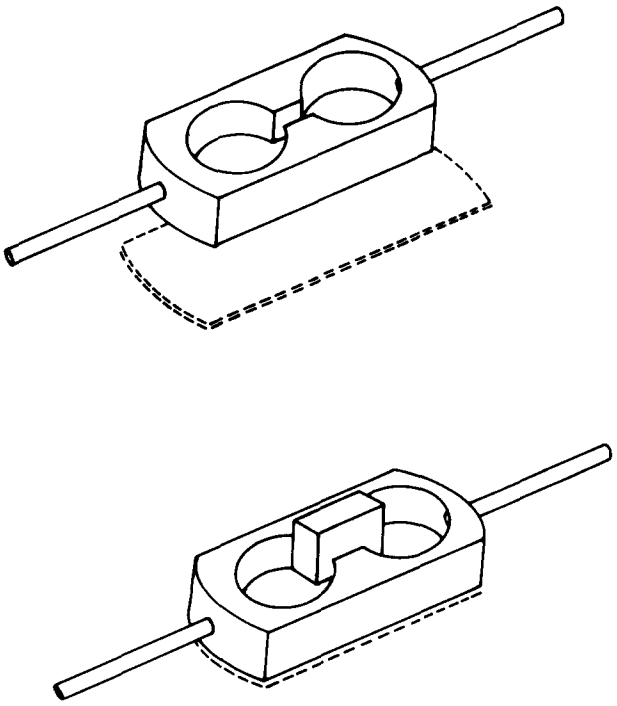

FIGURE 1 Modified Kamiya double chamber. The chambers were made from an acrylic block into which two 5/16″ holes were drilled out. The middle area between the holes has been drilled out and fitted with a stopper. The bottom was fitted with a no. 2 coverslip. Vent holes, 1/16″ have been drilled into the ends to which brass tubing has been attached. The stopper is removed during specimen preparation and the resulting vacant area filled with 2% agarose (Sigma Chemical Co.) (see text). This design of the chamber allows for polarized light examination of the endoplasm during experimentation.

Large particles (15–36 $\mu$m) were pulled magnetically in the $X$ direction at various forces. Regardless of force, there were no observable contrast changes to suggest strain or flow BR around the particle (33). Neither was a birefringent tail observed trailing the particle, as would be expected if the vacuole had long filaments associated with it. At this level of investigation, the membrane of the vacuole appears to be a good approximation for the shear surface of the particle.

### Yield Stress and Elasticity

The plasmodial vein was mounted with the long axis oriented vertically, so that both falling ball ($Y$ direction) (11, 38) and magnetic pull ($X$ direction) experiments were possible. The first parameter investigated was yield stress. Spheres less than ~3.7 $\mu$m in diameter did not displace with respect to a reference endoplasmic granule. Video records of this observation have been obtained in the neighborhood of 10 min. From this observation, a measure of the yield stress in the $Y$ direction, $\tau.y$, was calculated to be ~1.05 dyn/cm$^2$ (see APPENDIX).

[1] *Abbreviations used in this paper:* BR, birefringence.

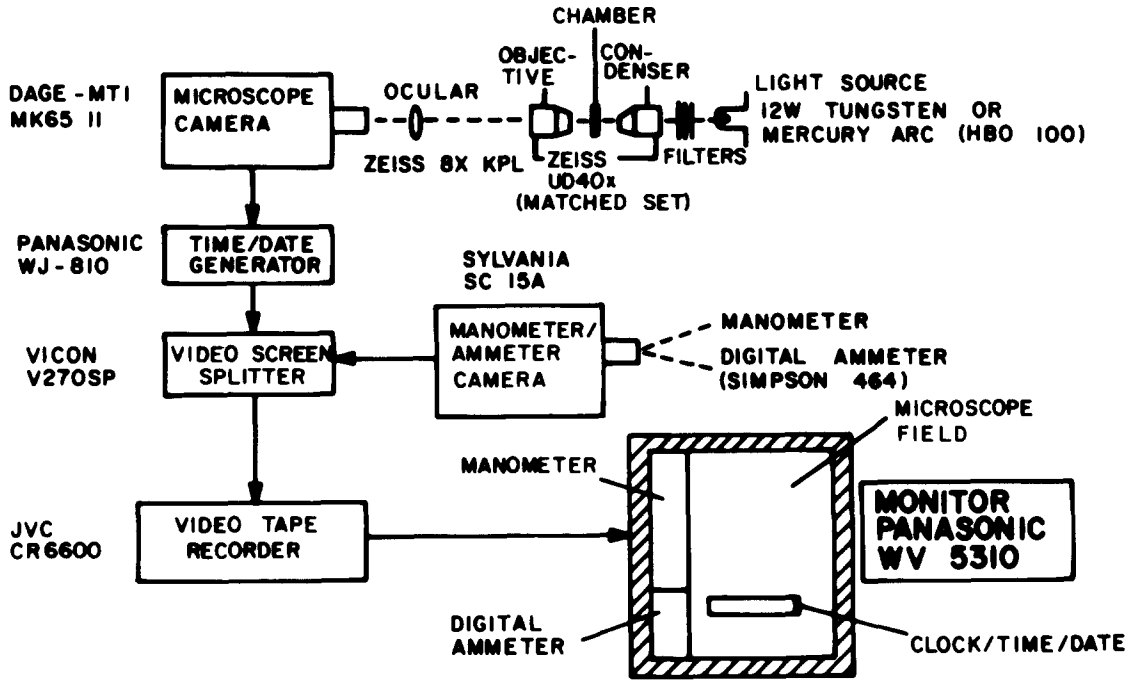


FIGURE 2 General layout of video components. Video components were assembled in a manner that allowed the simultaneous imaging of the manometer, ammeter, time, and microscopic field (110 $\mu$m wide) on the monitor screen. Note the positioning of the double chamber and the tubing attached to one side from the manometer.

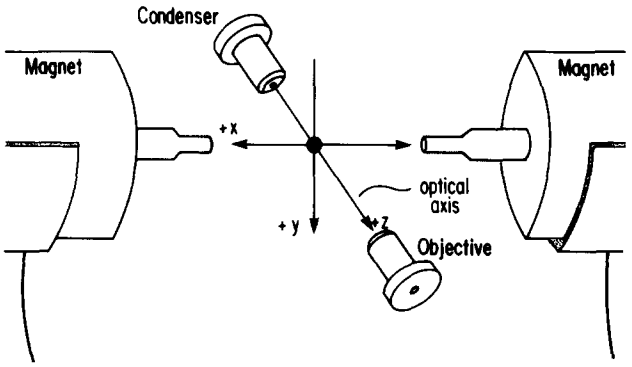


FIGURE 3 Coordinates. The origin ($X = Y = Z = 0$) is located as the specimen point as defined by the microscope. The horizontal axis defines the $X$ axis and coincides with the central axis of the magnetic pole pieces. $X$ increases toward the left calibrated magnet. The vertical axis (direction of gravity) defines the $Y$ axis. This direction is parallel to the long axis of the specimen. The $Z$ axis is defined by the optic axis of the microscope (see text).

Yield stress in the $X$ direction, $\tau$.x, was determined with the use of the magnet. By using the manometer, the endoplasm was kept as motionless as possible and a nonfalling magnetic sphere centered in the microscope field. In each experiment, the current to the left magnet was slowly increased until the sphere was perceived to permanently displace relative to a reference endoplasmic granule. This magnetic yield force was maintained for a time, and the trajectory of the particle was recorded on video tape.

Fig. 4 shows the trajectories of an initially stationary 2.9-$\mu$m diameter sphere magnetically pulled through successive regions of the endoplasm at consecutive times. In each case, the particle was pulled magnetically at the corresponding yield stress ($\tau$.x) for a time and then released. $\Delta$ is the trajectory of the sphere pulled with a magnetic force ($F_m$) of $6.57 \times 10^{-8}$ dyn from 29.58 min to 30.03 min after the preparation had been mounted onto the microscope. $\star$ is the trajectory with $F_m = 6.21 \times 10^{-8}$ dyn at 1.37 min after the last data point of $\Delta$. $\square$ is the trajectory with $F_m = 6.18 \times 10^{-8}$ dyn at 7.37 min after $\Delta$. The magnetic sphere was not pulled back to the point of origin in each successive experiment; and so, new endoplasm was sampled each time.

The marked variability and complex nature of these trajectories suggest that the endoplasm is not homogeneous. The endoplasm did reproducibly show the existence of a yield stress and a variable amount of elastic recoil upon termination of magnetic force. The values of the calculated yield stresses ($\tau$.x) are summarized in Table I (see Appendix for calculations). A mean value of $\tau.x = 0.58 \pm 0.1$ dyn/cm$^2$ was calculated.

Table I also lists the $F_m$ used to permanently displace a stationary particle in the $X$ direction. $F_y$ lists the force in the $Y$ direction already acting on the sphere as a consequence of $F_g$-$F_b$ (see Appendix). In every case but one, $F_y > F_m$; yet the particle was stationary in the $Y$ direction with respect to a reference granule before application of the smaller $F_m$. This is evidence for structural anisotropy.

## Apparent Viscosity

In the following experiments, magnetic spheres 4–16 $\mu$m in diameter were used in endoplasmic regions of 70–110 + $\mu$m in diameter. Trajectories of these larger spheres were less complicated and generally linear with time. Apparent viscosity of the endoplasm could be measured alternately in two directions, $X$ and $Y$, with the same magnetic sphere in the same region of the specimen. The sphere was first pulled across the vein with a known $F_m$. The resulting velocity ($u_x$) was used to obtain the uncorrected viscosity value. Ladenburg's end correction (36) was applied to generate the apparent viscosity value $\eta_x$ (see Appendix). The sphere was then

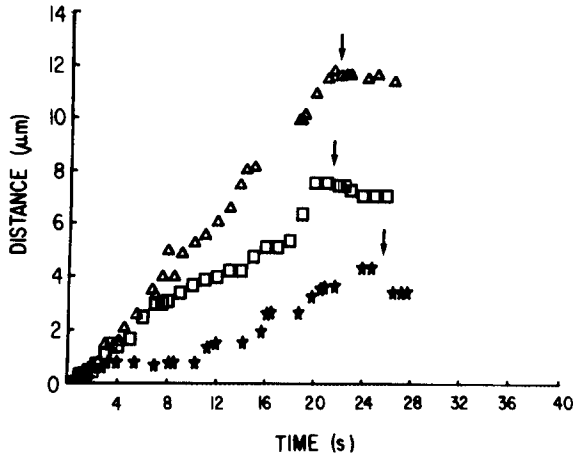


FIGURE 4 Comparative trajectories. Three sequential trajectories of an initially stationary 2.9-μm sphere in successive regions of the endoplasm. Δ was pulled with $F_m = 6.57 \times 10^{-8}$ dyn from 29.58 min to 30.03 min after the preparation was mounted onto the microscope. ☆ was pulled with a $F_m = 6.21 \times 10^{-8}$ dyn at 1.37 min after Δ. □ was pulled with $F_m = 6.18 \times 10^{-8}$ dyn at 7.37 min after Δ.

TABLE I

*Yield Stress Determination in the X Direction*

| Diameter | τ.x | $F_m$ | $F_y$ |
|---|---|---|---|
| μm | dyn/cm² | dyn | dyn |
| 2.0 | 0.56 | $3.06 \times 10^{-8}$ | $3.13 \times 10^{-8}$ |
| 2.0 | 0.53 | $2.93 \times 10^{-8}$ | $3.13 \times 10^{-8}$ |
| 2.5 | 0.78 | $6.70 \times 10^{-8}$ | $6.11 \times 10^{-8}$ |
| 2.5 | 0.65 | $5.62 \times 10^{-8}$ | $6.11 \times 10^{-8}$ |
| 2.7 | 0.39 | $3.95 \times 10^{-8}$ | $7.70 \times 10^{-8}$ |
| 2.8 | 0.52 | $5.56 \times 10^{-8}$ | $8.58 \times 10^{-8}$ |
| 2.8 | 0.64 | $6.89 \times 10^{-8}$ | $8.58 \times 10^{-8}$ |
| 2.9 | 0.57 | $6.57 \times 10^{-8}$ | $9.54 \times 10^{-8}$ |
| 2.9 | 0.54 | $6.21 \times 10^{-8}$ | $9.54 \times 10^{-8}$ |
| 2.9 | 0.54 | $6.18 \times 10^{-8}$ | $9.54 \times 10^{-8}$ |
| 3.3 | 0.73 | $1.09 \times 10^{-8}$ | $1.41 \times 10^{-8}$ |
| 3.3 | 0.68 | $1.01 \times 10^{-8}$ | $1.41 \times 10^{-8}$ |
| 3.3 | 0.61 | $9.15 \times 10^{-8}$ | $1.41 \times 10^{-8}$ |
| 3.3 | 0.61 | $9.08 \times 10^{-8}$ | $1.41 \times 10^{-8}$ |
| 3.9 | 0.44 | $9.24 \times 10^{-8}$ | $2.32 \times 10^{-7}$ |

Mean: 0.58 ± 0.13

Initially stationary magnetic spheres were displaced in the *X* direction by slowly increasing *I* to the left magnet. $F_m$ lists the magnetic force necessary for this perceived permanent displacement. τ.x lists the corresponding calculated yield stress in the *X* direction. $F_y$ lists the force already on the sphere in the *Y* direction, as a result of $F_g - F_b$ before application of $F_m$.

roughly centered with respect to the vein and allowed to fall (falling ball viscometry [11, 38]). The resulting velocity ($u_y$) was used to generate the Faxen corrected (14) apparent viscosity ($\eta_y$) (see Appendix). A dynamoplasmogram was generated for 10 min after the last viscosity measurement. All of the viscosity vs. time points and dynamoplasmograms (Fig. 5, *A* and *B*) were fitted to a curve using a cubic spline algorithm (21). The actual data points are denoted as *x*.

Fig. 5*A* is a plot of $\eta_x$ (solid line) and $\eta_y$ (dashed line) with respect to time (44.85–948.9 s). The $\eta_x$ and $\eta_y$ values were observed to fluctuate but were not regular enough to warrant the calculation of a period. The dynamoplasmogram (Fig. 5*B*) was started 3.3 s after the last data point of the $\eta_y$ plot and exhibits a period of 90 s as calculated for six cycles. Attempts were made to correlate the frequency of the dynamoplasmogram (Fig. 5*B*) with that of the fluctuating viscosity plots (Fig. 5*A*); no correlations could be deduced, although such possibilities seemed appealing over short time intervals.

The interdependence between $\eta_x$ and $\eta_y$ was tested by calculating the linear correlation coefficient ($r_{xy}$) between these two plots. To examine the possibility of a phase relationship between the $\eta_x$ and $\eta_y$ curves, coefficients were calculated for the $\eta_x$ curve shifted from 50 s behind to 50 s ahead of the $\eta_y$ plot. The resulting plot of correlation coefficient vs. shift revealed a curve that fluctuated about zero. This asserts that $\eta_x$ and $\eta_y$ were independent of each other over the tested interval.

## *Shear Stress vs. Rate of Shear*

The shear over the surface of a sphere traveling through a medium is not homogeneous (54), precluding direct calculation of shear stress and rate of shear. For this reason, the parameters $F/d^2$ and $u/d$ were employed instead. Shear stress is defined as force per unit area; therefore, $F/d^2$ should be proportional by a geometrical correction factor. Rate of shear is defined as the change in velocity of flow with distance perpendicular to the direction of flow. In the case of a sphere, diameter was the only depth measure available; and so, $u/d$

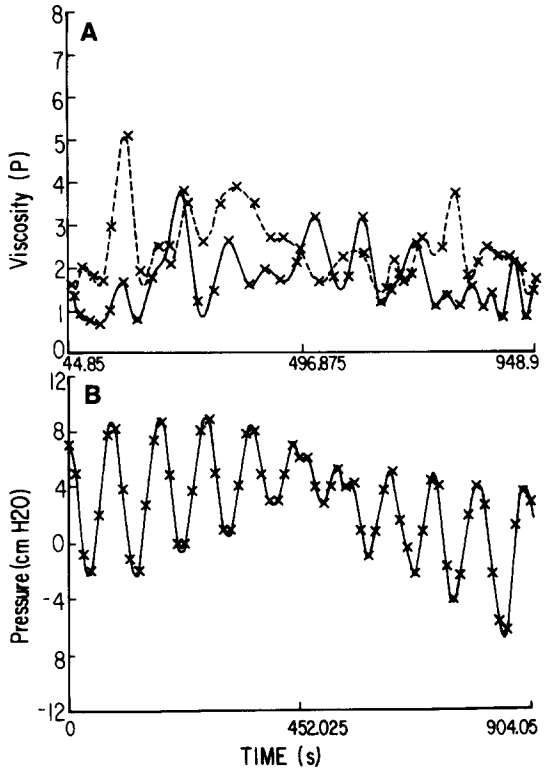


FIGURE 5 Apparent viscosity of the endoplasm. (*A*) The solid line refers to the change in apparent viscosity with time across the specimen ($\eta_x$) as measured with the magnetic viscoelastometer (see text). The dashed line refers to the apparent viscosity parallel to the specimen long axis ($\eta_y$) as measured with the falling ball technique. The two sets of data were generated alternately over the same time period with the same magnetic sphere in the same organism. (*B*) A dynamoplasmogram was generated for 904.05 s, 3.3 s after the last data point of the $\eta_y$ plot. A period of 90 s was calculated for six shuttle streaming cycles. In both figures, the real data points are represented by x. All plots were fitted to a cubic spline algorithm.

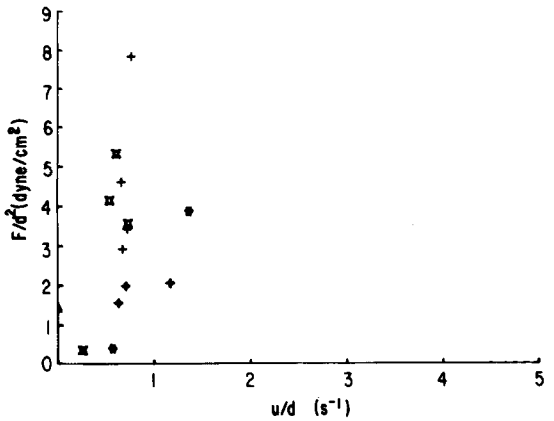


FIGURE 6 Shear stress ($F/d^2$) vs. rate of shear ($u/d$) plot derived in the Y direction with the falling ball technique (see text). The symbols refer to the various specimens used. Each point refers to a mean calculated from several measurements. Different shear stresses were applied by using different sized spheres in the same sample. The Y intercept (△) was calculated from the yield stress ($\tau_y$ = 1.05 dyn/cm²). A Newtonian fluid would exhibit linear behavior from the origin in this plot.

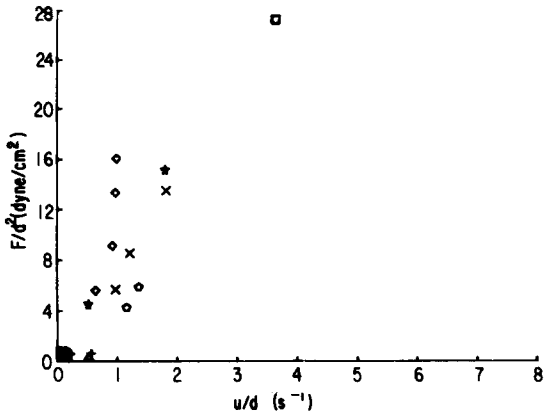


FIGURE 7 Shear stress ($F/d^2$) vs. rate of shear ($u/d$) plot derived in the X direction with the magnetic viscoelastometer. Each symbol corresponds to a specific sphere pulled across the endoplasm at varying $F_m$ (see text). Each point refers to a mean calculated from several measurements. Spheres ☆, □, and ⬠ were also measured in the same organism.

was used for rate of shear, again subject to geometrical correction.

Plots of $F/d^2$ vs. $u/d$ were generated by the falling ball method (Y direction) and magnetic particle method (X direction). In the falling ball method, shear stress was varied by changing the diameter of the sphere. Measurements were taken in the same specimen with successive spheres having different diameters (Fig. 6). In the X direction, shear stress was varied in the same specimen with the same sphere by changing the $F_m$ on the sphere (Fig. 7). An attempt was made to derive a complete range of data for each specimen.

In Fig. 6, each symbol refers to the same specimen in which several different sized spheres were used. Each point refers to a mean calculated for several measurements obtained with a sphere. The Y intercept (△) was calculated from the estimated yield stress ($\tau$.y = 1.05 dyn/cm²). In Fig. 7, each symbol refers to a specific sphere pulled in the X direction at various $F_m$. Spheres ☆, □, and ⬠ were also used successively in the same specimen. Each point corresponds to a mean calculated for several measurements performed with a specific sphere at each $F_m$. The smudge of data points in the lower left of Fig. 7 refers to experiments performed at and just above the yield stress ($\tau$.x) for that specimen. The raw data for Figs. 6 and 7 are available in Sato (48).

Figs. 6 and 7 show that a simple relationship between shear stress ($\tau$) and rate of shear ($\dot{\gamma}$) does not exist for the endoplasm. These experiments were characterized by a remarkable variability in the measured data (48). What is clear, however, is that the endoplasm is non-Newtonian and not a shear thinning material (30). The form of the curves (Figs. 6 and 7) beyond the Y intercept may actually suggest a shear thickening behavior of the endoplasm (19, 46).

## DISCUSSION

### Magnetic Rheometry

Our magnetic particle technique represents an improvement over past efforts for several reasons. First, the relatively large distance between the pole piece and specimen results in a constant magnetic force across the entire microscope field, a condition not established in previous efforts. This has been confirmed with gaussmeter measurements. Second, the coils are cooled with refrigerated water to optimize their current carrying capability. When combined with the large pole piece to specimen distance, the cooling ensures minimal heating of the specimen by the magnet. Third, the power supply is current-regulated, eliminating variations in magnetic force due to changes in coil resistance. Fourth, centration through the microscope permits precise pole piece to specimen alignment to within ±5 μm. Fifth, the microscopic probe size produces a minute shear stress, resulting in minimal disruption of endoplasmic structure. The size also allows the detection of regional heterogeneities. Finally, the two magnets allow the experimenter to maneuver the sphere away from the ectoplasm. This area is filled with plasmalemmal invaginations (1, 13, 47, 55) and is therefore prone to artifact. Measurements were taken in the mid 80% region of the endoplasm as observed in streaming veins before experimentation.

### Rheological State of Endoplasm

Kamiya (26) has presented evidence that the endoplasmic streaming is the passive result of a local difference in internal pressure generated by contraction of the ectoplasmic wall. Kamiya and Kuroda (29) represented the velocity profile of the endoplasm as a truncated parabola. This implies that the inner core of endoplasm flows as an unsheared, homogeneous plug at low to moderate streaming rates. In other words, the general endoplasmic rheology is a function of flow. We present evidence that the situation is much more complex and that a truncated paraboloid velocity profile does not adequately describe the rheology of the endoplasm.

Measurements of yield stress, apparent viscosity, and elasticity were not very reproducible with time (Figs. 4–7). These fluctuations have been shown to occur in the same vein with the same sphere, force, and temperature. In all cases, the endoplasm was held as motionless as possible with balance pressure. In Fig. 5A and B, the frequency content of the dynamoplasmogram was compared with that of the $\eta_x$ and $\eta_y$ plots. These viscosity fluctuations appear to occur independently of the shuttle streaming cycle, and therefore seem to be

independent of flow. Linear correlation coefficient analysis between the $\eta_x$ and $\eta_y$ plots showed that they also fluctuate independently of each other.

The rationale for the treatment of the apparent viscosity data depicted in Fig. 5*A* was to test the notion that the endoplasm may be responding to changes in concentration of factors, such as calcium and ATP, which have been shown to affect the polymerization of cytoskeletal proteins (52). Calcium, ATP, membrane potential, birefringent filaments, heat production, and contractile activity have all been shown to oscillate in relation to the shuttle streaming cycle (5, 22, 27, 28, 31, 43, 51, 57, 58). A calcium-sensitive actin polymer fragmenting protein, fragmin, has recently been isolated from plasmodium (17). A 36-kdalton actin-binding protein that aggregated microfilaments has also been identified in *Physarum* (44). The interaction between these proteins and/or factors with actin may be involved in the regulation of the rheological properties of the endoplasm.

The above notion implies that the endoplasm is a fairly homogeneous material, but this is probably not the case. The minimum acceptable translation of a sphere at 1 s after the application of current ($I$) was 10 $\mu$m. Spheres traversing long distances, 40 $\mu$m and more, were occasionally seen to exhibit velocity changes. Originally, these data were assumed to be spurious. However, these velocity changes were occasionally observed to occur over the mid portion of the vein. On change of focus, the endoplasm appeared homogeneous with no obstructions visible. The velocities recorded gave no support for the existence of a gradient of properties either parallel or perpendicular to the vein (3). Therefore, an alternative interpretation of Figs. 4–7 is that the endoplasm is composed of heterogeneous domains that were randomly sampled. The observed velocity shifts suggest that this latter interpretation is more likely. This would explain the variability of the data and its indifference to the motility cycle.

However, the reproducible existence of yield stress and elastic recoil in the endoplasm is highly suggestive of the existence of structure or structures. The force relationship in Table I indicates a structural anisotropy to the endoplasm. Both of these points and the existence of a negative BR in the endoplasm (43) support the notion of organization, i.e. a cytoskeleton. Little information is available at present, however, as to its form or character in vivo.

Kasai et al. (32) and Maruyama et al. (39) showed that actin polymer solutions exhibit shear thinning behavior. This is interesting because as much as 20% of the total protein content of *Physarum* can be actin, depending on the stage (34, 41). However, $F/d^2$ (stress) vs. $u/d$ (rate of shear) plots (Figs. 6 and 7) in *Physarum* show that the endoplasm is not a shear thinning material in the $X$ and $Y$ directions as expected (30), but may be shear thickening, instead. If actin molecular interactions are the basis of the endoplasmic rheology, the modulation of this structural protein in vivo appears to be far more complex than has been successfully modeled to date in vitro.

The behavior of the endoplasm at higher shear stresses has yet to be characterized. The data presented here are characteristic of the whole endoplasm, i.e., macrorheological (45). No information is available on the contribution to the measurements by the membranes, granules, soluble macromolecules, or polymerized elements (if any, see references 25, 42).

Measurements of particle displacement in these creep experiments have been taken with respect to the smallest discernible granules in the endoplasm, on the assumption that granules do not move with respect to the ground substance of endoplasm. There is some evidence to the contrary; Mustacich and Ware (40) have evidence for submicroscopic materials in *Physarum* that exhibit behavior significantly different from that of endoplasmic granules. Also, lateral drift between a reference granule and another granule in stilled endoplasm could approach 0.2 $\mu$m/s. Our measurements usually took ~8 s; clearly, however, there is room for improvement.

### Corrections

The adequacy of the various corrections (C [38], Faxen [14], Ladenburg [36]) used in the derivation of the rheological values (apparent viscosity, yield stress, rate of shear) has not been substantiated when applied to non-Newtonian viscoelastic fluids. The values of the parameters presented may be subject to additional correction. Therefore, greater emphasis has been placed on the behavior of these parameters as a function of time, region, and shear stress than on the numerical values themselves.

## CONCLUSION

A promising technique for the in vivo characterization of cells has been presented. In these experiments, the maximum temporal resolution was ~30 s. The organism has been shown to be capable of significantly changing its rheological properties within this time period (see also reference 49) or is composed of heterogeneous domains. The endoplasm of *Physarum polycephalum* has been shown to be a structurally anisotropic, non-Newtonian, viscoelastic fluid with a yield stress.

## APPENDIX

This appendix describes in detail the instrumentation and calculations involved in the derivation of apparent viscosity and yield stress. The section includes a discussion of the magnetic rheometer calibration and the choice of magnetic particles. A preliminary error analysis of the technique is also described.

### Magnetic Rheometer

Annealed Hy Mu 80052 particles were used in this investigation (Carpenter Technology, Reading, PA). These particles are spheroidal in shape, possess high magnetic permeability, and are not harmful to the organism (48, 49).

The Hy Mu 800 spheres were pulled by magnets located on either side of the specimen (Fig. 3). Each of the two magnets consists of two coils (~900 turns of 19 AWG wire) wound onto a single water-cooled aluminum spool, and wired in parallel (50). The pole pieces were machined from 1.27-cm diameter moly permalloy 80 rod (Carpenter Technology), and annealed (Allegheny Ludlum Steel Corp., Brackenridge, PA) after fabricating the tips (Fig. 3). The pole piece tips (4 mm diameter) are 1.2 cm from the specimen point. Both magnets are mounted on an optical bench for precise alignment through the microscope. The magnets are driven by a 6274B regulated DC power supply (Hewlett Packard, Lexington, MA) in the current regulated mode. This supply can provide up to 60 V at 15 A.

## Magnetic Force Determination

The force ($F_m$) on a magnetic sphere of volume $V$, subjected to a magnetic field ($B$) is:

$$F_m = K' V B \frac{dB}{dx}, \quad (1)$$

where $K'$ is a constant (see below).

The magnetic rheometer was calibrated in two steps. First, the magnetic field parameters $\left(B, \frac{dB}{dx}\right)$ were determined as a function of magnetic current, $I$. Second, $F_m$ was measured on sample spheres in an oil viscosity standard (380.1cP, 25°C, Cannon Instrument Co., State College, PA) to determine $K'$.

The magnetic field was measured directly using a Bell 640 gaussmeter (Bell Inc., Columbus, OH). These measurements confirmed that the magnetic flux density ($B$) and its gradient $\left(\frac{dB}{dx}\right)$ are linear functions of $I$ at the specimen point. Further measurements demonstrated that $B$ and $\frac{dB}{dx}$ did not vary appreciably even 2 mm off axis. Therefore, $F_m$ is constant across the microscope field. Since $B$ and $\frac{dB}{dx}$ are each linearly related to $I$, the product $B\frac{dB}{dx}$ can be described by a quadratic equation of the form:

$$\hat{B}\frac{d\hat{B}}{dx} = a_2 I^2 + a_1 I + a_0, \quad (2)$$

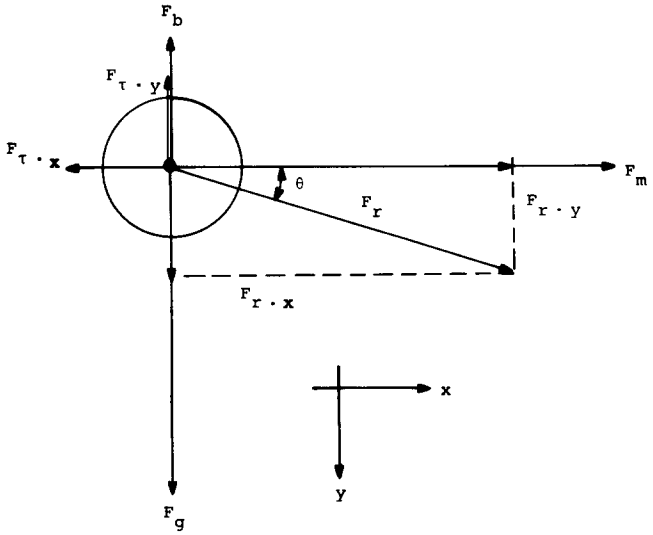


FIGURE 8 Force balance on a sphere. $F_g$(gravitational force) = $\frac{4\pi r^3 \rho_b g}{3}$. $F_b$(bouyant force) = $\frac{4\pi r^3 \rho_m g}{3}$. $F_r$(resultant drag force) = $6\pi r\eta u$. $F_m$(magnetic force) = $1.185 \times 10^2(2.2045I^2 + 23.490I + 24.541)r^3$. $F_{\tau,x,y}$(yield force) = $\tau_{x,y}\pi r^2 C$. The variables are: $r$(cm) = radius of the sphere, $\rho_b$ = density of the sphere (8.74 g/cm³), $g$ = acceleration due to gravity (980 cm/s²), $\rho_m$(g/cm³) = density of medium, $\tau_{x,y}$(dyn/cm²) = yield stress in $X$ or $Y$ direction, and $C$ = geometrical correction for shear around a sphere (1.75 [38]). Yield forces exist only in the organism.

where $a_2$, $a_1$, and $a_0$ are constants characteristic of the electromagnet at a fixed point in space. $\hat{B}\frac{d\hat{B}}{dx}$ is the predicted value of $B\frac{dB}{dx}$. Note that $a_0$ may be non-zero due to residual magnetism in the pole piece.

The product $B\frac{dB}{dx}$ was calculated as a function of $I$, and a least-squares quadratic fit was used to determine the coefficients $a_2$, $a_1$, and $a_0$. For the left magnet used in all of our measurements, we found $a_2 = 2.2045 \times 10^2$, $a_1 = 2.3490 \times 10^3$, and $a_0 = 2.4541 \times 10^3$. These constants, when used in equation (2) with $I$ in amperes, yield $\hat{B}\frac{d\hat{B}}{dx}$ in gauss²/cm.

$K'$ is a constant which is governed by the physical and magnetic properties of the magnetic particles. $F_m$ was determined by allowing a particle to fall in the viscosity standard (Cannon Instrument Co.) and measuring the deflection angle $\theta$ (Fig. 8). From Fig. 8, Eq. 3 can be derived:

$$F_m = (F_g - F_b)\cot\theta, \quad (3)$$

where $F_g - F_b = (\rho_b - \rho_m)gV$.

Here, $V$ is the particle volume, $\rho_b$ is the density of the particle (8.74g/cm³), $\rho_m$ is the density of the surrounding fluid, and $g$ is the gravitational acceleration (980 cm/s²).

Equating (3) and (1), the following expression for $K'$ can be derived:

$$K' = \frac{(\rho_b - \rho_m)g\cot\theta}{\hat{B}\frac{d\hat{B}}{dx}}$$

$$= \frac{(\rho_b - \rho_m)g\cot\theta}{(a_2 I^2 + a_1 I + a_0)}.$$

For simplicity, let $K = \frac{\cot\theta}{(a_2 I^2 + a_1 I + a_0)}$.

Then: $$K' = K(\rho_b - \rho_m)g$$

The constant $K$ was evaluated by measuring $\theta$ at various magnet currents, $I$. The temperature of the sample was maintained at 25.0 ± 0.1°C by a temperature-controlled circulating water bath (model K2, Messgerate-Werk Lauda, Brinkman Instruments, Westbury, NY). Experiments were recorded on video for subsequent analysis. The slope $K$ was calculated for each of five particles by a linear regression of cot $\theta$ to $B\frac{dB}{dx}$. For the Hy Mu 800 particles, we found $K = (3.67 \pm 0.35) \times 10^{-5}$ cm/gauss². These particles have a density of 8.74 g/cm³, and the viscosity standard has a density of 0.8739 g/cm³. Therefore:

$$K' = K(\rho_b - \rho_m)g = 0.2829 \text{ g/cm s}^2 \text{ gauss}^2.$$

The magnetic force (dynes) on a given sphere of radius ($r$) in cm is:

$$F_m = K' V B \frac{dB}{dx} = (0.2829)\left(\frac{4}{3}\pi r^3\right)(a_2 I^2 + a_1 I + a_0),$$

where $I$ is the input current in amperes.

## Viscosity and Yield Stress Calculations

From Fig. 8, the force balance on a falling ball in a Newtonian fluid of infinite extent becomes Stokes' Law:

$$F_f = F_g - F_b$$

$$\text{or:} \quad \eta = \frac{2r^2 g(\rho_b - \rho_m)}{9u}$$

In the organism with a sphere falling parallel to the long axis of the vein:

$$F_f = F_g - F_b - F_{\tau.y}$$

$$\text{thus:} \quad \eta = \frac{2r^2 g(\rho_b - \rho_m)}{9u} - \frac{\tau.rC}{6u}.$$

The density of the endoplasm has been estimated to be 1.12 g/cm$^3$ (Belcher, unpublished observations, and reference 37). Spheres having diameters of 3.7 $\mu$m or less were observed not to fall in the $Y$ direction with respect to endoplasmic granules. A measure of the yield stress, $\tau$.y, was calculated by letting $F_f = 0$ because of zero flow:

$$F_g = F_{\tau.y} + F_b$$

$$\tau.y = \frac{4rg(\rho_b - \rho_m)}{3C}$$

$$\tau.y = 1.05 \text{ dyn/cm}^2$$

Faxen's correction was used to account for ectoplasmic wall effects in the organism (14):

$$\eta_y = \frac{\eta}{1 - 2.108\frac{r}{R_c} + 2.09\left(\frac{r}{R_c}\right)^3 - 0.95\left(\frac{r}{R_c}\right)^5}$$

$\eta_y$ is defined as the Faxen-corrected apparent viscosity in the $Y$ direction, where $r$ and $R_c$ are the radii of the sphere and vein, respectively.

In in vivo magnetic experiments, the following force relationship occurs on a sphere being pulled across the vein (Fig. 8):

$$F_f = F_m - F_{\tau.x}$$

With $F_f = 0$, the endoplasm was found to have a yield stress in the $X$ direction ($\tau$.x) of 0.58 ± 0.1 dyn/cm$^2$ (see Results). With flow ($F_f \neq 0$):

$$\eta = \frac{6.2898(2.2045I^2 + 23.490I + 24.541)r^2 - 0.1692r}{u}$$

Ladenburg's correction was used to account for ectoplasmic end effects (36):

$$\eta_x = \frac{\eta}{1 + 3.3\frac{r}{h}}$$

$\eta_x$ is defined as Ladenburg's corrected apparent viscosity in the $X$ direction with radius ($r$) in cm and length of the tube ($h$) in cm.

## Variability of Magnetic Rheometry

A $\cot\theta$ vs. $B\frac{dB}{dx}$ plot was generated for five spherical particles in viscosity standard (Cannon Instrument Co.). The average slope was $3.666 \times 10^{-5}$ gauss$^2$/cm. The standard deviation of the slope was $0.35 \times 10^{-5}$ gauss$^2$/cm which corresponds to a ±10% error between particles in a Newtonian fluid. This probably reflects the heterogeneities in composition between particles, which become important in determining magnetic properties at this scale.

The authors would like to thank Dr. Y. Hiramoto, Tokyo Institute of Technology; Dr. M. King, McGill University; Dr. R. Cone, Johns Hopkins University; Dr. T. D. Pollard, Johns Hopkins University; Dr. M. Litt, University of Pennsylvania; and Dr. G. B. Wallis, Dartmouth College, for valuable discussions and demonstrations. Dr. T. B. Roos and Dr. J. E. Walsh, also of Dartmouth, kindly provided some of the necessary equipment. Finally, we'd like to acknowledge the technical assistance of K. A. Orndorff and D. T. Brown.

This work was supported by a research grant (GM-27284) from the National Institute of Health, Bethesda, Maryland, Administered by R. D. Allen.

*Received for publication 17 December 1982, and in revised form 10 June 1983.*

## REFERENCES

1. Achenbach, F., W. Naib-majani, and K. Wohlfarth-Bottermann. 1979. Plasmalemma invaginations of *Physarum* dependent on the nutritional content of the plasmodial environment. *J. Cell Sci.* 36:355–359.
2. Allen, R. D. 1960. The consistency of amoeba cytoplasm and its bearing on the mechanism of ameboid movement. *J. Biophys. Biochem. Cytol.* 8:379–397.
3. Allen, R. D. 1965. Rheological properties of slime mold endoplasm. *In* Symposium on Biorheology. A. L. Copley, editor. Interscience Publishers, New York. 173–174.
4. Allen, R. D., and N. S. Allen. 1983. Video-enhanced microscopy with a computer frame memory. *J. Microsc.* 129:3–17.
5. Allen, R. D., W. R. Pitts, D. Speir, and J. Brault. 1963. Shuttle-streaming: synchronization with heat production in slime mold. *Science (Wash. DC).* 142:1485–87.
6. Bennett, H. S. 1961. Methods applicable to the study of both fresh and fixed materials. *In* McClung's Handbook of Microscopical Techniques. R. M. Jones, editor. Hafner Publishing Co., Inc., New York. 591–695.
7. Brewer, E. N., and A. Prior. 1976. A simplified growth medium for *Physarum polycephalum. Physarum Newsletter.* 8:45.
8. Brown, D. E. S., and D. A. Marsland. 1936. The viscosity of amoeba at high hydrostatic pressure. *J. Cell Comp. Physiol.* 8:159–165.
9. Chambers, R., and E. L. Chambers. 1961. Explorations into the Nature of the Living Cell. Harvard Univ. Press, Cambridge, MA. 10–18, 228–278.
10. Crick, F. H. C., and A. F. W. Hughes. 1950. The physical properties of cytoplasm: a study by means of the magnetic particle method, I, II. *Exp. Cell Res.* 1:37–39, 505–533.
11. Cygan, D. A., and B. Caswell. 1971. Precision falling sphere viscometry. *Trans. Soc. Rheol.* 15:663–683.
12. Daniel, J. W., and H. H. Baldwin. 1964. Methods of culture for plasmodial myxomycetes. *In* Methods in Cell Physiology I. D. M. Prescott, editor. Academic Press, New York. 9–41.
13. Daniel, J. W., and U. Jarlfors. 1972. Plasmodial ultrastructure of the myxomycete *Physarum polycephalum. Tissue & Cell.* 4:15–36.
14. Faxen, H. 1922. Die Bewegung einer starren Kugel langs der Achse eines mit zaher Flussingkeit gefullten rohres. *Ark. Mat. Astron. Fys.* 17:1–28.
15. Goodman, E. M. 1980. *Physarum polycephalum*: A review of a model system using a structure-function approach. *Int. Rev. Cytol.* 63:1–58.
16. Harvey, E. N., and D. A. Marsland. 1932. The tension at the surface of *Amoeba dubia* with direct observations on the movement of cytoplasmic particles at high centrifugal speeds. *J. Cell Comp. Physiol.* 2:75–97.
17. Hasegawa, T., S. Takahashi, H. Hayashi, and S. Hatano. 1980. Fragmin: a calcium ion sensitive regulatory factor on the formation of actin filaments. *Biochemistry* 19:2677–2683.
18. Heilbronn, A. 1922. Eine neue Methode zur bestimmung der Viskositat lebender Protoplasten. *Jahrb. Wiss. Bot.* 61:284–38.
19. Heilbrunn, L. V. 1956. The Dynamics of Living Protoplasm. Academic Press, New York. 25–27.
20. Hiramoto, Y. 1969. Mechanical properties of the protoplasm of the sea urchin egg. *Exp. Cell Res.* 56:201–208.
21. Hornbeck, R. W. 1975. Numerical Methods. Quantum Publishers, N.Y. 47–50, 80–106, 121–129.
22. Hulsmann, N., and K. E. Wohlfarth-Bottermann. 1978. Spatio-temporal relationships between protoplasmic streaming and contraction activities in plasmodial veins of *Physarum polycephalum. Cytobiologie.* 17:317–34.
23. Hwang, S. H. 1967. Viscoelastic Behavior of Biological Fluids. Ph.D. Thesis, Univ. of Pennsylvania.
24. Inoué, S. 1981. Video image processing greatly enhances contrast, quality and speed in polarization-based microscopy. *J. Cell Biol.* 89:346–356.

25. Isenberg, G., and K. E. Wohlfarth-Bottermann. 1976. Transformation of cytoplasmic actin. *Cell Tissue Res.* 173:495–528.
26. Kamiya, N. 1940. The control of protoplasmic streaming. *Science (Wash. DC).* 92:462–463.
27. Kamiya, N. 1959. Protoplasmic streaming. *Protoplasmatologia.* 8,3a. 1–199.
28. Kamiya, N. 1981. Physical and chemical basis of cytoplasmic streaming. *Annu. Rev. Plant Physiol.* 32:205–36.
29. Kamiya, N., and K. Kuroda. 1958. Studies on the velocity distribution of the protoplasmic streaming in the myxomycete plasmodia. *Protoplasma.* 49:1–4.
30. Kamiya, N., and K. Kuroda. 1973. Dynamics of cytoplasmic streaming in a plant cell. *Biorheology.* 10:179–187.
31. Kamiya, N., Y. Yoshimoto, and F. Matsumura. 1981. Physiological aspects of actomyosin-based cell motility. *In* International Cell Biology ('80–'81). H. G. Schweiger, editor. Springer-Verlag, Berlin. 346–358.
32. Kasai, M., H. Kawashima, and F. Oosawa. 1960. Structure of F-actin solutions. *J. Polym. Sci. Part D Macromol Rev.* 64:51–69.
33. Kasai, M., and F. Oosawa. 1972. Flow birefringence. *Methods Enzymol.* 26:289–323.
34. Kessler, D., V. T. Nachmias, and A. G. Loewy. 1976. Myosin content of *Physarum* plasmodia and detection of immunological cross reactions with myosins from related species. *J. Cell Biol.* 69:393–406.
35. Komnick, H., W. Stockem, and K. E. Wohlfarth-Bottermann. 1973. Cell motility: mechanisms in protoplasmic streaming and amoeboid movement. *Int. Rev. Cytol.* 34:169–249.
36. Ladenburg, R. 1907. Uber den EinfluB von Wanden auf die Bewegung einer Kugel in einer reivenden Flussingkeit. *Ann. Phys. (Leipzig).* 23:447.
37. Leontjew, H. 1928. Zur Biophysik der niederen Organismen. *Z. Vgl. Physiol.* 7:195–200.
38. MacLean-Fletcher, S. D., and T. D. Pollard. 1980. Viscometric analysis of the gelation of *Acanthamoeba* extracts: purification of two gelation factors. *J. Cell Biol.* 85:414–428.
39. Maruyama, K., M. Kaibara, and E. Fukada. 1974. Rheology of F-actin I. Network of F-actin in solution. *Biochim. Biophys. Acta.* 371:20–24.
40. Mustacich, R. V., and B. R. Ware. 1977. Study of protoplasmic streaming in *Physarum polycephalum* with laser doppler spectroscopy. *Protoplasma.* 91:351–367.
41. Nachmias, V. T. 1979. The contractile proteins of *Physarum polycephalum* and actin polymerization in plasmodial extracts. *In* Cell Motility: Molecules and Organization. S. Hatano, H. Ishikawa, and H. Sato, editors. Univ. of Tokyo Press, Tokyo. 33–57.
42. Nagai, R., and I. Kato. 1975. Cytoplasmic filaments and their assembly into bundles in *Physarum* plasmodium. *Protoplasma.* 86:141–158.
43. Nakajima, H., and R. D. Allen. 1965. The changing pattern of birefringence in plasmodia of the slime mold, *Physarum polycephalum. J. Cell Biol.* 25:361–374.
44. Ogihara, S., and Y. Tonomura. 1982. A novel 36,000 dalton actin-binding protein purified from microfilaments in *Physarum* plasmodia which aggregates actin filaments and blocks actin-myosin interaction. *J. Cell Biol.* 93:604–614.
45. Reiner, M. 1956. Phenomenological macrorheology. *In* Rheology, Theory and Applications Vol. 1. F. R. Eirich, editor. Academic Press, New York. 9–62.
46. Reiner, M. 1960. Deformation, Strain and Flow. H. K. Lewis and Co., London. 306–310.
47. Rhea, R. 1966. Electron microscopic observations on the slime mold *Physarum polycephalum* with specific reference to fibrillar structures. *J. Ultrastruct. Res.* 15:349–379.
48. Sato, M. A Rheological Investigation of Living Cytoplasm. Hanover, New Hampshire: Dartmouth College, 1983. Ph.D. thesis.
49. Sato, M., T. Z. Wong, and R. D. Allen. 1983. A preliminary rheological investigation of living *Physarum* endoplasm. *In* The Application of Laser Light Scattering to the Study of Biological Motion. J. C. Earnshaw and M. W. Steer, editors. Plenum Publishing Corp., New York. 389–402.
50. Seifriz, W. 1924. An elastic value of protoplasm with further observations on the viscosity of proptoplasm. *Br. J. Exp. Biol.* 3:1–12.
51. Takeuchi, Y., and M. Yoneda. 1977. Synchrony in the rhythm of the contraction-relaxation cycle in two plasmodial strands of *Physarum polycephalum. J. Cell Sci.* 26:151.
52. Taylor, D. L. 1976. Motile model systems of amoeboid movement. in Cell Motility (vol.B). R. Goldman, T. Pollard, and J. Rosenbaum, editors. Cold Spring Harbor Laboratory, Cold Spring Harbor, NY. 797–821.
53. Taylor, D. L., and J. S. Condeelis. 1979. Cytoplasmic structure and contractility in amoeboid cells. *Int. Rev. Cytol.* 56:57–144.
54. Van Wazer, J. R., J. W. Lyons, K. Y. Kim, R. E. Colwell. 1963. Viscosity and Flow Measurement: A Laboratory Handbook of Rheology. Interscience Publishers, N.Y. 272–276.
55. Wohlfarth-Bottermann, K. E. 1974. Plasmalemma invaginations as characteristic constituents of plasmodia of *Physarum polycephalum. J. Cell Sci.* 16:23–37.
56. Yagi, K. 1961. The mechanical and colloidal properties of amoeba protoplasm and their relations to the mechanism of amoeboid movement. *Comp. Biochem. Physiol.* 3:73–91.
57. Yoshimoto, Y., and N. Kamiya. 1978. Studies on contraction rhythm of the plasmodial strand III. Role of endoplasmic streaming in synchronization of local rhythms. *Protoplasma.* 95:111–121.
58. Yoshimoto, Y., F. Matsumura, and N. Kamiya. 1981. Simultaneous oscillations of $Ca^{+2}$ efflux and tension generation in the permealized plasmodial strand of *Physarum. Cell Motility.* 1:433–443.